This manuscript has been published as:
Katrin Vu, Ming-Che Lee, Gerhard Blankenburg, Yun-Ru Chen, Ming-Lee Chu, Andreas Erbe, Leonardo Lesser-Rojas, Yun-Ru Chen, Chia-Fu Chou: Time-evolved SERS signatures of DEP-trapped Aβ and Zn^{2+}Aβ peptides revealed by a sub-10 nm electrode nanogap. *Analytical Chemistry*, **93**, 16320-16329 (**2021**). DOI: 10.1021/acs.analchem.1c01521

This work was selected as supplementary cover art of issue 49/2021 of Analytical Chemistry.

Final published version of the manuscript is available from:
https://10.1021/acs.analchem.1c01521

Time-evolved SERS signatures of DEP-trapped Aβ and Zn^{2+}Aβ peptides revealed by a sub-10 nm electrode nanogap

Katrin H. P. Vu[†,#,‡], *Ming-Che Lee*[§,‖], *Gerhard H. Blankenburg*[†,‡,○], *Yu-Jen Chang*[‖,Δ], *Ming-Lee Chu*[‡], *Andreas Erbe*[◊], *Leonardo Lesser-Rojas*[□,¶], *Yun-Ru Chen*[§,‖]* *and Chia-Fu Chou*[‡,⊥]*

[†]Nanoscience and Technology Program, Taiwan International Graduate Program, Academia Sinica, Taipei 11529, Taiwan, R.O.C.

[#]Department of Engineering and System Science, National Tsing Hua University, Hsinchu 30013, Taiwan, R.O.C.

[‡]Institute of Physics, Academia Sinica, Taipei 11529, Taiwan, R.O.C.

[§]Graduate Institute of Life Sciences, National Defense Medical Center, Taipei 11490, Taiwan, R.O.C.

[‖]Genomics Research Center, Academia Sinica, Taipei 11529, Taiwan, R.O.C.

[○]Department of Physics, National Taiwan University, Taipei 10617, Taiwan, R.O.C.

[Δ]Taiwan International Graduate Program in Interdisciplinary Neuroscience, National Taiwan University and Academia Sinica, Taipei 11529, Taiwan, R.O.C.

[◊]Department of Materials Science and Engineering, NTNU, Norwegian University of Science and Technology, NO-7491 Trondheim, Norway

□Research Center for Atomic, Nuclear and Molecular Sciences, San Pedro de Montes de Oca, San Jose 11501, Costa Rica

¶School of Physics, University of Costa Rica, San Pedro de Montes de Oca, San Jose 11501, Costa Rica

⊥Research Center for Applied Sciences, Academia Sinica, Taipei 11529, Taiwan, R.O.C.

KEYWORDS: Surface-enhanced Raman spectroscopy (SERS), amyloid-β (Aβ), dielectrophoresis (DEP), electrode nanogap

ABSTRACT: Alzheimer's disease (AD) has become extensively relevant in ageing societies, yet the fundamental molecular basis for AD is still poorly understood. New tools to study the undergoing structural conformation changes of amyloid beta (Aβ) peptides, the pathogenic hallmark of AD, could play a crucial role in the understanding of the underlying mechanisms of misfolding and cytotoxicity of this peptide. It has been recently reported that Zn^{2+} interacts with Aβ and change its aggregation pathway away from less harmful fibrillar forms to more toxic species. Here, we present a versatile platform based on a set of sub-10 nm nanogap electrodes for the manipulation and sensing of biomolecules in physiological condition at low copy number, where molecules are trapped via dielectrophoresis (DEP) across the nanogap, which also serves as a SERS hotspot. In this study, we demonstrate that our electrode nanogap platform can be used to study the structural difference between Aβ40 and ZnAβ40 peptides at different aggregation stages in the physiologically-relevant concentration, and in solution phase. The Raman spectroscopic signatures of the DEP-captured neuropeptides prove the device to be attractive as a label-free bioanalytical tool.

Alzheimer's disease (AD) is the most common form of dementia in the elder population after age of 65.[1] This neurodegenerative disorder is causing an increasing economic and social impact due to longer life expectancy and the increase of such population.[2] Thus, the treatment for AD has become more and more relevant, yet failure of clinical trials suggest that the fundamental molecular mechanism of AD pathogenesis is still not fully understood.[3] The prevalent explanation of the cause of AD is the amyloid hypothesis, postulating the fundamental role of amyloid beta (Aβ) peptides in the development of the disease.[4] Aβ peptides, which are natural products of metabolism, consist of 39-42 amino acids and are the major constituents of senile plaques in the brains of Alzheimer's disease patients.[5] However, it has been found that the soluble Aβ oligomeric species, formed during the early stage of misfolding and aggregation of non-toxic Aβ monomers to insoluble β-sheet rich fibrils, were more cytotoxic than the final fibrillar form of Aβ.[6, 7] Aβ is further known to bind with metal ions, such as Zn^{2+}, Cu^{2+}, Fe^{3+} and Al^{3+}.[8, 9] Those metal ions were found to interact with histidine residues at the N-terminus of the peptide.[10] Dyshomeostasis of metal ions, including Zn^{2+}, Cu^{2+}, Fe^{3+} and Al^{3+}, has been linked with AD pathology.[8, 9] It has been shown in previous studies that the presence of metal ions has distinct effects on the kinetic pathway of Aβ aggregation. While Cu^{2+}, Fe^{3+} and Al^{3+} promote the formation of amorphous aggregates[11-13], Zn^{2+} was reported to form oligomeric species[13] with increased cytotoxicity.[3, 14]

Knowledge of the structure of the different Aβ species would be helpful in further understanding the underlying mechanisms of misfolding and cytotoxicity, requiring appropriate tools. Techniques commonly used for the structural analysis of proteins include X-ray diffraction, nuclear magnetic resonance (NMR), circular dichroism (CD), Fourier transform infrared spectroscopy (FTIR) and Raman spectroscopy. Aβ is a natively unfolded protein and does not crystallize which makes X-ray diffraction and solution NMR studies problematic.[6] Raman

spectroscopy is a non-invasive technique that is able to determine protein structures in physiological conditions even for disordered structures, and for which light absorption by water is not a limiting factor.[15] It can be used to characterize proteins in various states, precipitated fibrils, amorphous aggregates, solids and crystals.[16] One major drawback of this technique is the low Raman scattering cross-section of most biomolecules. Raman enhancement techniques using plasmonic nanostructures, such as SERS and TERS, can overcome this problem by providing enhancement up to 14 orders of magnitude compared with non-resonant Raman spectroscopy.[17, 18] While resonance Raman enhancement offers the possibility to probe selectively with high sensitivity regions around certain chromophores, SERS/TERS enhancement can enhance spectral features of entities in a "hot spot" independent on their molecular composition.[19, 20]

Other challenges in characterizing biomolecules lie in preparation, isolation and stability of the sample, as this might have an impact on the result. Sample isolation is usually a critical factor as the molecules of interest are often present only in trace amounts.[21] Molecular diffusion also adds to the challenge: while unperturbed molecular conformation in solution is preferred for analysis, Brownian motion tends to prevent the molecules from getting to the SERS hotspot.

In this work, we have addressed these issues by developing a platform for the manipulation and sensing of biomolecules in physiological conditions. This device features an array of nanogap electrode pairs that enable trapping of molecules via dielectrophoresis[22-30] as well as nanoantenna-enhanced Raman detection[31-33]. This work extends the performance of a platform previously developed by our group[34] by increasing the Raman enhancement capability of the nanoantennae by adding a plasmonic enhancement from gold substrate. This improved platform is then used to study conformational differences of Aβ peptides upon interaction with zinc ions.

RESULTS

Figure 1 shows the design of our nanogap device and a schematic diagram of the experimental setup can be found in the Supporting Information (Figure S1). The device contains 15 pairs of Ti/Au microelectrodes each extends in between with one pair of Ti/Au nanowire electrodes. The array of electrodes is arranged in three groups, each consisting of five identical electrode pairs. The groups differ by the internal angle of the nanoelectrode tips, namely 40˚, 60˚ and 80˚. For simplicity, the tip angle used in experiments is assumed to be 60˚, unless specified. The size of the interelectrode distance used for the experiment ranged between 5-15 nm. In contrast to our previous work, we used a Ti/Au double layer instead of Ti as material for the nanoelectrodes since Au is widely known for its superior plasmonic enhancement properties.[35]

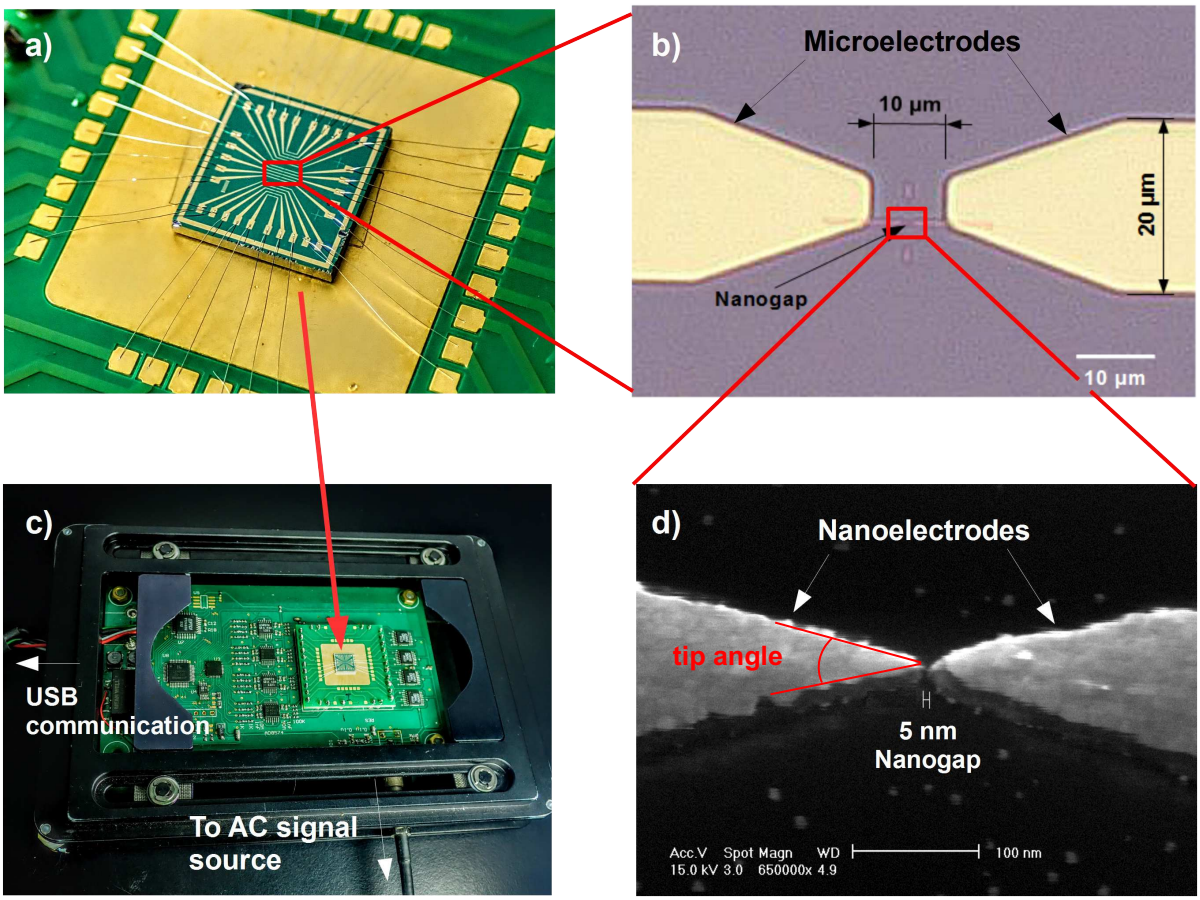

Figure 1. (a) Wire-bonded chip (7 x 7 mm) with 15 pairs of Au electrodes. (b) Optical microscopy image of one pair of microelectrodes and nanoelectrodes. (c) Our sensing system on a custom-made printed circuit board. (d) SEM image of the electrode nanogap (tilted view).

In order to find the experimental conditions and field parameters for the DEP trapping of Aβ peptides, we performed experiments with fluorophore-labelled Aβ and monitored the process using fluorescence microscopy. For larger, β-sheet rich aggregates, such as Aβ fibrils, ThT fluorescent dye was used, while smaller species with much less β-sheet structures were labelled with FAM fluorescent dye. In our setup, Aβ fibrils were successfully trapped with a DEP field frequency of 1 MHz while for Aβ oligomers a frequency of 3 MHz was appropriate. In all cases, Aβ peptides were only trapped above a threshold of 10 V_{PP} for the electric field amplitude. Because of the short range of the DEP interaction (~ µm), trapping occurred rapidly and reached saturation within seconds (Figure 2). To show the reversibility of the trapping process, we performed

experiments where we switched the AC field on and off in intervals of 10 seconds (Movies S1 and S2). Figure S3 in the Supplementary Information shows the time course of the fluorescence intensity during those cycles of DEP trapping, indicating the reversible trapping/operation of the device.

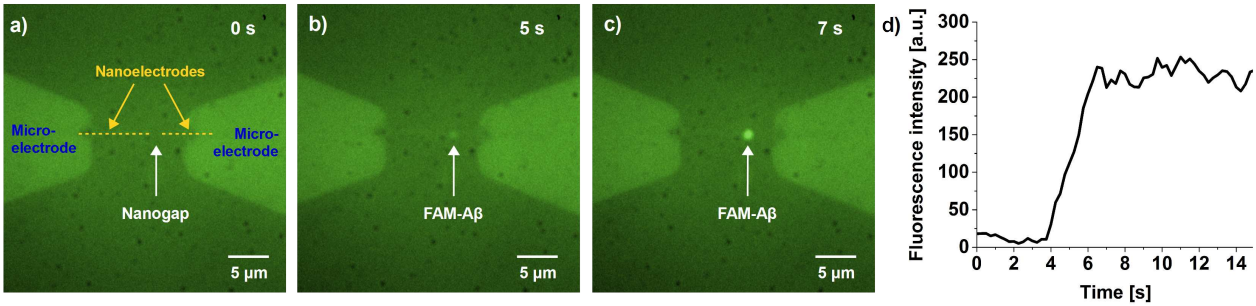

Figure 2. Fluorescence microscopy images of FAM-labelled-Aβ oligomers trapped inside the nanogap after (a) 0 s, (b) 5 s and (c) 7 s of AC field application (see Movies S1 and S2 in SI); (d) Fluorescence intensity vs. time of Aβ oligomer trapping inside the nanogap. Fluorescence images were running-averaged over 5 frames. AC field parameters: 3 MHz, 15 V_{PP}; and peptide concentration was 500 nM.

In order to locate and confirm the position of the nanogap for Raman measurements, spectral maps were taken (Figure S2a-c). In a spectral map acquired without baseline correction, a region of high intensity was identified after integrating over the luminescence background, revealing the position of the Raman hotspot. As described and explained in our previous paper, the luminescence is enhanced in the vicinity of the metal nanogaps due to increased excitation intensity consistent with an electromagnetic mechanism.[34] A Raman map integrated over the Amide III region (1225 – 1280 cm^{-1}) confirms that peptides are being trapped and their Raman spectra are enhanced in the very same hotspot (Figure S2c).

A concentration of 50 µM was used to grow the samples; for Raman experiments, samples were diluted to an initial monomer concentration of 50 nM. We used the same dilution for all samples, implying that after aggregation the final concentration of oligomers and fibrils is expected to be

much lower than 50 nM. However, only a rough estimation can be given for the concentration for the oligomeric and fibril species because they vary in size (see Lee et al. [3] for the size distribution of ZnAβ). For example, ZnAβ after 100 hrs of incubation has a molecular weight ranging from 152 to 214 kDa (~33- to 49-mer), so the concentration is expected to be between 1 and 1.5 nM, allowing a low-copy number detection.

We have measured the Raman signature of Aβ40 at different aggregation stages, namely after 0 h, 43 h, 79 h and 144 h incubation time. According to the well-established aggregation characteristics of amyloid peptides, at 0 h the monomeric state dominates; at 43 h, in the lag phase, the oligomeric state is more noticeably present than in other stages; After 79 h, in the elongation phase, the fibril formation is happening at its highest rate; and after 144 h, an equilibrium state (plateau phase) is reached that is dominated by fibrils.[36] This is consistent with our observations (Figure 3a). Figure 3b-c shows a comparison of Raman spectra of Aβ at those four aggregation stages in the presence and absence of Zn^{2+}, with each Raman spectrum being a cumulative spectrum of three individual SERS spectra in order to show most of the bands but at the same time not using too many spectra as this might obstruct the visibility of the bands of interest. Temporal fluctuations frequently encountered in SERS spectra stem from the diffusion of single molecules occupying several conformations and orientations at the probing site[37]. Large proteins such as Aβ fibrils can only fit partly into a small enhanced active volume ($\sim$ few nm^3); thus, SERS measurements may probe only a few building blocks, namely amino acids, thereby leading to unavoidable spectral fluctuations[37]. However, this was not a problem in our case as Aβ fibrils are formed by a repeated structure of beta-sheet stacked monomers. For large proteins with less homogenous structure, with different parts producing different Raman signatures, a larger number of spectra would be necessary to probe the whole molecule with our setup.

Raman bands, listed in Table 1, were assigned on the basis of existing literature and typically consist of vibrational modes from amide bands and aromatic as well as non-aromatic amino acid side chain residues.[38-44]

Table 1. Assignment of bands in SERS spectra of Aβ.

Raman shift (cm^{-1})	Assignment	References
1000	Phe	20, 21, 22
1036	Phe	20, 21
1144	C-C-N stretching	20
1235-1245	amide III (β-sheet)	20, 21, 22
1264-1279	amide III (α-helix)	20, 21, 22
1455	CH_2 deformation	20, 23
1574	Stretching vibration of histidine imidazole ring	24
1600	Phe, Zn-histidine	23, 24
1640-1654	amide I (α-helix)	25, 26
1665-1680	amide I (β-sheet)	25, 26

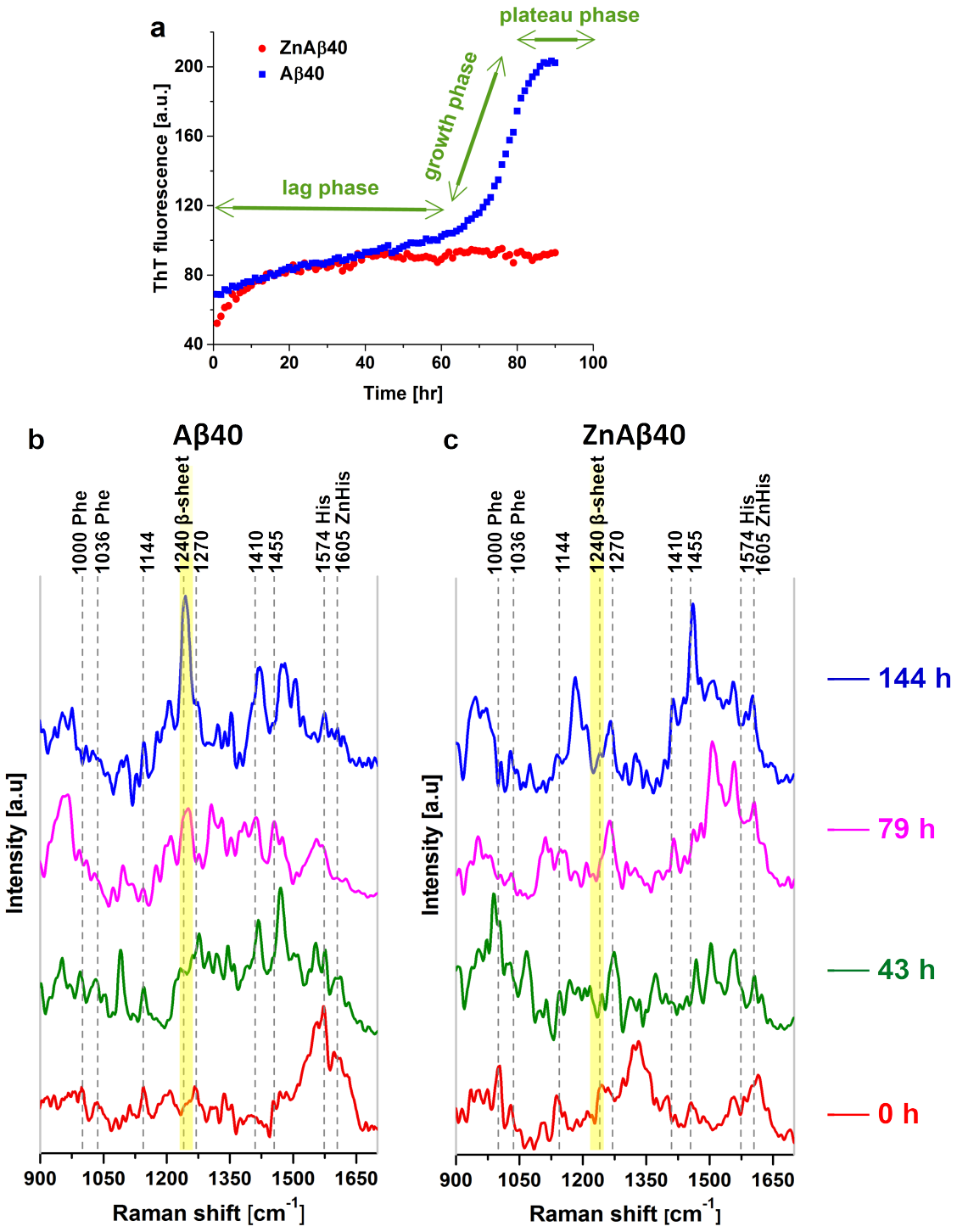

Figure 3. (a) ThT fluorescence assay. SERS spectra of Aβ40 in solution trapped with the nanogap device (b) without Zn^{2+} and (c) with Zn^{2+} after 0 h, 43 h, 79 h and 144 h, respectively. The amide III β-sheet mode at 1240 cm^{-1} is highlighted (yellow bars). Peptide concentration was 50 nM (as per Aβ monomer) for Raman experiment and 50 μM for ThT assay. Raman spectra were normalized to the intensity of the C-C-N stretching mode at 1144 cm^{-1}. Spectra were background subtracted, each averaged over three spectra, and offset vertically for better visibility.

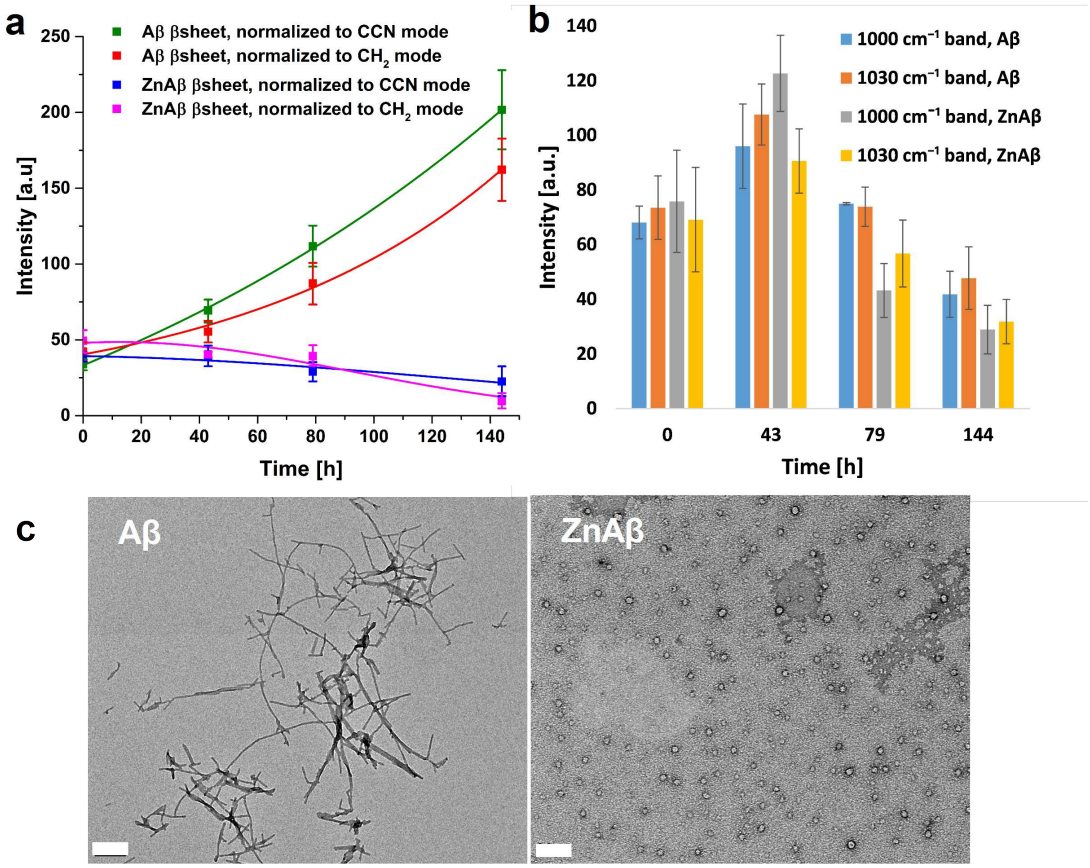

Figure 4. Analysis of peak height versus time of Aβ40 in the presence and absence of Zn^{2+} for: (a) the amide III β-sheet band at 1240 cm^{-1} in aqueous solution normalized to the C-C-N stretching mode at 1144 cm^{-1} and the CH_2 bending mode at 1455 cm^{-1}, respectively (exponential curve fitting was performed). (b) Phe bands at 1000 cm^{-1} and 1030 cm^{-1}. (c) TEM images of the end-point products of Aβ alone or ZnAβ. The scale bars are 100 nm.

With increasing incubation time, as shown in Figure 3b, a band appeared in the amide III region at around 1240 cm^{-1} with a higher intensity, which was identified as an indicator for β-sheet formation according to Table 1. In contrast, we observed a low intensity of the band at 1240 cm^{-1} (Figure 3c) throughout the samples incubated with Zn^{2+}. These changes in the Raman intensity of the β-sheet bands are shown in Figure 4a, with the intensities being normalized to bands which do not depend on conformation, such as the CCN stretching mode at 1144 cm^{-1} and the CH_2 bending mode at 1455 cm^{-1}.[45] Similar tendencies in the changes of the normalized intensity can be seen in both cases. In addition, the Raman signature of Aβ and ZnAβ was measured in dried state on our nanogap chip, likewise showing a decreased intensity of the 1240 cm^{-1} band for the Zn^{2+} incubated

sample (Figure 5). We observed strong bands in the amide I region (1640-1680 cm^{-1}) for dried Aβ samples. The amide I mode consists of C=O stretching and C-N stretching vibrations.[43, 46] Interestingly, no obvious bands were observed for samples in solution. Possible reasons for this observation will be discussed later. Furthermore, Thioflavin T (ThT) assays were performed, as shown in Figure 3a. A significantly higher increase in ThT fluorescence was observed in the absence of Zn^{2+}, as compared to the presence of Zn^{2+}, in which case the ThT signal was retained without much increase.

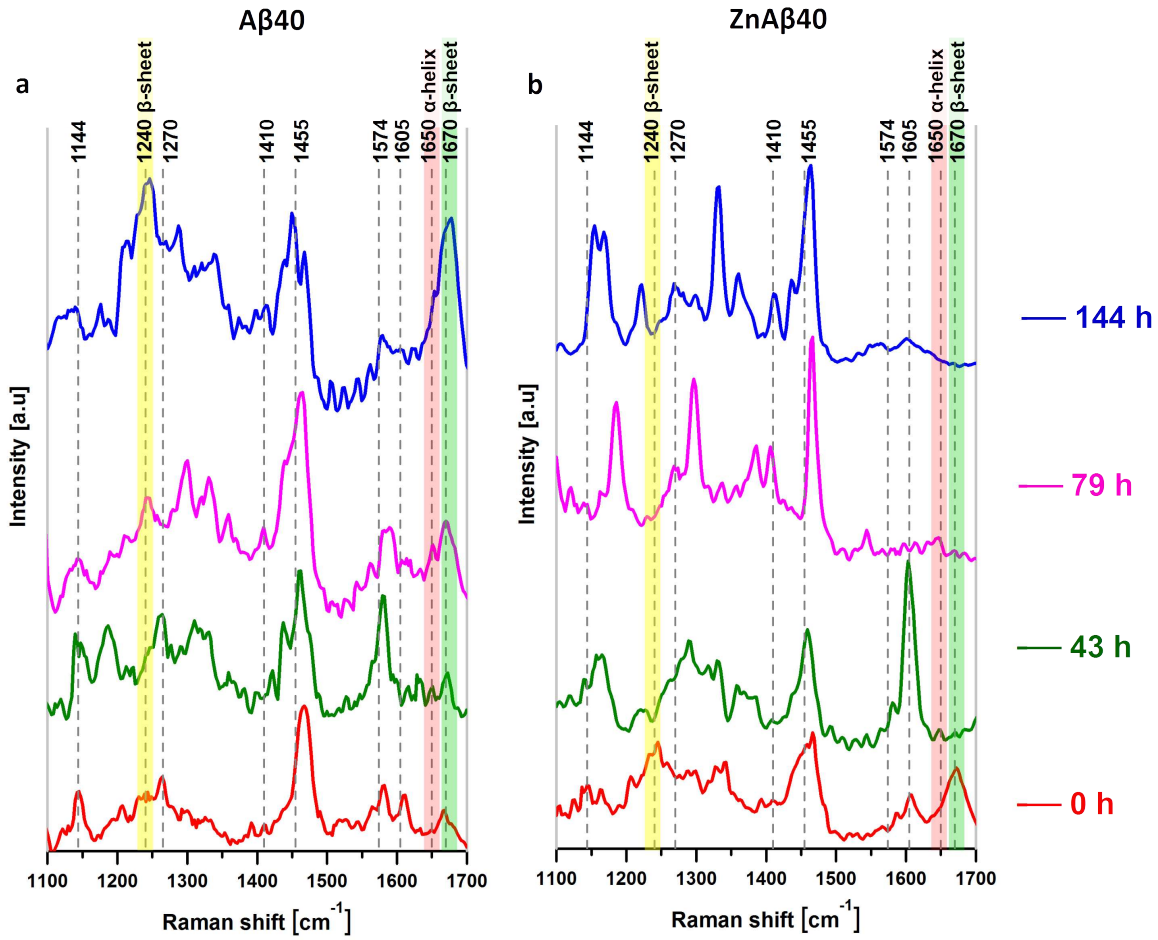

Figure 5. SERS spectra of Aβ40 in dried phase (a) without Zn^{2+} and (b) with Zn^{2+} after 0 h, 43 h, 79 h and 144 h, respectively. The amide III β-sheet mode at 1240 cm^{-1} is highlighted (yellow bars) as well as the amide I modes at 1650 and 1670 cm^{-1} (red and green bars). Raman spectra were normalized to the intensity of the C-C-N stretching mode at 1144 cm^{-1}. Spectra were background subtracted, each averaged over three spectra, and offset vertically for better visibility.

Further, a band at 1574 cm^{-1} was observed, which can be assigned to the C_4=C_5 stretching vibration of the imidazole ring of histidine. This mode has been reported to shift upon binding of Zn^{2+} from 1574 to 1605 cm^{-1},[42] where a phenylalanine band originally resides. Such frequency upshift is found in all ZnAβ samples (Figure 3c), supporting previous reports of histidine being the main binding site for Zn^{2+}.[42]

DISCUSSION

Fluorescent signal fluctuations

With the field parameters and peptide concentration used in our fluorescence experiments, the signal usually reaches saturation within a few seconds (Fig. 2). In SERS experiments, however, the signal plateaus in roughly two minutes (Fig. S6). This is due to the fact that a higher peptide concentration (500 nM) was used for fluorescence observations than for SERS measurements (~1 – 50 nM).

While it is obvious from Fig. 2d that trapping equilibrium is reached quickly, it can be seen in Fig. S3 that the overall fluorescence intensity as well as the intensity fluctuations vary significantly between each cycle of DEP trapping. We would like to point out that the mechanism of DEP trapping is fully reversible, and the trapping efficiency of the electrodes remains unchanged after repeated trapping cycles. In contrast, we ascribe the observed fluctuations to two effects. On one hand, this is due to photobleaching, since the illuminated area exceeding the image boundaries, or field of view, ($d > 40$ μm) is much larger than the bright spot around the DEP hotspot that was integrated for signal analysis ($d \approx 2$ μm), such that molecules present in the surrounding areas

outside the trapping volume are also subject to photobleaching. On the other hand, the statistical nature of a low-copy-number trapping experiment with a non-uniform sample also plays a role.

In our previous publication[34], we demonstrated the low-copy number of protein detection capability of our technology. The DEP trapping volume is defined as the space within which the DEP force is strong enough to overcome the effect of diffusion so that any molecule immediately gets trapped into the DEP hotspot, and it can be determined for a known uniform sample[47]. Equilibrium is reached when the concentration gradient is high enough to generate a rate of diffusion directed outward of the trapping volume equal to the rate of inward diffusion. Once equilibrium is reached, molecules enter and leave the DEP hotspot at equal rates, and the number of trapped molecules observed at any given time follows a Poisson distribution. Since we aim to keep the expected value of that statistics low, higher relative fluctuations of the fluorescence intensity are observed, like in FCS or other single-molecule like experiments[48-50].

Considering another sample with similar dielectric properties but a different uniform particle size, the Stokes-Einstein equation implies that larger particles take a longer time to diffuse into or out of the trapping volume and reach equilibrium than smaller particles. The DEP force in turn scales with the volume of the target particle[22], effectively increasing the size of the trapping volume for larger particles compared to smaller ones. We may therefore observe that smaller target particles quickly reach an equilibrium of trapping rate and escape rate, while larger target particles continue to accumulate in the hot spot for a longer time.

The FAM-Aβ sample used for recording fluorescent videos has a non-uniform oligomer size distribution with unknown number density distribution. The sample is tagged with one fluorescent marker per monomer, so that larger oligomers appear brighter than smaller ones. As explained

above, the timescale to reach equilibrium as well as the size of the trapping volume are expected to vary significantly for oligomers of different sizes. On one hand, the time evolution of the fluorescent signal reflects the counting statistics of the number of trapped molecules in a state of equilibrated trapping and escaping rates within a given ensemble. On the other hand, the particular composition of all the oligomers located within trapping distance from the electrode nanogap at any given time fluctuates as well, even after reaching a steady state, and in the regime of low copy-number trapping, these fluctuations may be obvious on large timescales, giving the impression that the DEP trap becomes more or less effective over time, which is not the case.

Raman spectroscopy analysis

The amide III band (1200-1300 cm^{-1}), one of the most informative parts of the protein Raman spectrum regarding secondary structure, is associated with C-N stretching, N-H bending and C-C stretching of the peptide group;[16] amide bands which originate from such polypeptide backbone vibrations have been correlated to different secondary structural conformations of proteins.[51, 52] In this work, the band associated with β-sheets around 1240 cm^{-1} was interpreted to indicate β-sheet formation in Aβ peptides in the absence of Zn^{2+}, in contrast to inhibited β-sheet formation in the presence of Zn^{2+}. This interpretation is further supported by ThT assay results (Figure 3a). Since this fluorophore displays enhanced fluorescence upon binding to β-sheet rich structures,[53] a clearly growing signal upon incubation in the absence of Zn^{2+} implies evident β-sheet formation, while a stagnating signal in the presence of Zn^{2+} indicates suppressed β-sheet formation, leading to the conclusion that Zn^{2+} inhibits the formation of β-sheet-rich fibrils. This claim is backed by TEM images of the aggregated amyloids (Figure 4c). These findings are consistent with the work of Lee et al., reporting that even after 6 days of incubation the CD spectra of Aβ with Zn^{2+} did not show evident β-sheet signature, whereas Aβ40 without Zn^{2+} readily formed β-sheet fibrils.[3] Our results

also corroborate the picture that the native-like secondary structure of the monomeric peptide in the absence of Zn^{2+} is converted to β-sheet rich fibrils during the aggregation process, as established by other reports.[38, 39] To prove that the effect of Zn^{2+} prohibiting the formation of fibrils is not a charge induced effect but an ion-specific effect, we measured the Raman spectra of Aβ trapped in solution using our nanogap device, as well as in dried state in the presence of Mg^{2+}, which has the same charge as Zn^{2+}, after 0 h and 144 h incubation. The results in Figures S4 and S5 show a significant increase in β-sheets after 144 h, indicating fibril formation, as in the Zn^{2+}-free scenario, clearly indicating the ion-specific effect.

For SERS measurements, mostly 5 or 6 nm gap sizes were used for Aβ samples without Zn^{2+}, while for Aβ samples with Zn^{2+}, the gap sizes ranged from 6 to 15 nm. Given though the variation of the gap size due to the fabrication difficulties for their exact reproduction, it does not alter the overall trend of β-sheet formation as indicated in Fig. 4a, where the variation (error bars) of the peak height for the β-sheet signal of ZnAβ samples is small compared to that of the Aβ samples, regardless of the larger variation in gap size (6 – 15 nm).

In addition to the amide III band, the signature of phenylalanine has been analyzed as an independent indicator for aggregation processes. The results for Aβ both in the absence and presence of Zn^{2+} show that the phenylalanine bands at 1036 cm^{-1} and 1000 cm^{-1} exhibit a significant Raman intensity decrease as incubation time exceeds 43h (Figure 4b), where Aβ in the presence of Zn^{2+} showed a greater extent of decrease. In the case of Aβ without Zn^{2+}, this may be explained by fibril formation: As explained in the previous paragraph, our results of the amide III band analysis indicate in accordance with literature that in the absence of Zn^{2+}, Aβ undergoes fibril formation in which amino acids 16 to 20 (KLVFF) that forms a β-stand is crucial in fibril stacking[54]. In the cases of insulin and lysozyme, amyloid fibrils have been linked to an increased

appearance at the surface and exposure to the surrounding solvent of phenylalanine[55, 56], while Xu et al. have demonstrated that phenylalanine yields a reduced Raman signal when in contact with water.[57] In analogy to these papers, we attribute the decreased presence of phenylalanine in the Raman signature to its exposure to the surrounding water. In the presence of Zn^{2+}, the development of the Amide III band intensity suggests no fibril formation. However, the phenylalanine Raman band intensity after more than 43h incubation time is not stationary, but further decreased even more than the case of Aβ without Zn^{2+}. This indicates that the phenylalanine residues are increasingly exposed to water. Since two phenylalanine residues in Aβ are located in the core region of Aβ fibrils, the result reflects the conformational change caused by non-fibrillar aggregation of ZnAβ leading to exposure of the essential fibril core segment. These findings again support the claim by Lee et al. that ZnAβ forms large soluble aggregates but no fibrils.[3]

Although amide I bands could be clearly observed in the SERS spectra of dried Aβ samples, they were absent from some of the ZnAβ spectra (43, 79 and 144 hours). A number of cases of amide I mode suppression in SERS and TERS of various proteins (in dried phase) can be found in the literature.[46, 51, 52, 58, 59] In bulk confocal Raman spectroscopy, however, the amide I mode is always being observed in both dried state[16, 41, 46, 59] and solution.[42, 44, 59, 60] Consequently, amide I absence is a SERS/TERS-specific phenomenon; the exact reason for it is under debate. Blum et al. consistently observed a suppression of amide I bands in all their STM-TERS and SERS spectra, ruling out a possible electromagnetic shielding effect of the side chains.[46] On the other hand, it has been reported that the electrically enhanced Raman intensity decays exponentially by a factor of 2.3 to 10 per nm.[61] This close proximity effect might be even stronger if electrochemical interactions are taken into account.[51] Aβ monomers have a cross-section of 635 $Å^2$ or more,[62] which under the assumption of a roughly spherical particle gives a diameter of several nanometers.

This means that the molecular subdomains nearest to and farthest from the region of high field at the hotspot might experience enhancement factors that differ by several orders of magnitude, giving a plausible explanation for a decrease of certain Raman bands below the detection limit, if the originating structure is highly localized at the molecular surface. In the region of the hotspot, the intensity of a mode is determined by both the localization in the hotspot, and the orientation of the molecular element and its accompanying Raman tensor, as well as the polarization of the incoming light. This work will not elaborate further on these aspects due to lack of appropriate experimental data and it is beyond the scope of the current study.

Another possible explanation more specifically for the weakening of amide I bands could be the binding of several side chains to the Zn^{2+}, forcing the peptide backbone into a highly strained conformation, which does not produce a narrow Raman signature like relaxed monomers and β-sheet forming structures do. It is known that an increase in fraction of ordered backbone structure during formation of β-sheet and α-helix leads to an increase and sharpening of the amide I band compared to protein in a random coil conformation.[63] It seems plausible that a strain of Zn^{2+} embedding alters the protein structure in a way that would lead to a further decrease and broadening of the amide I signal up to the point where it cannot be detected any more.

A possible reason for "missing" amide I signals in case of solution samples might be an orientational effect during DEP trapping: peptides in solution that are dielectrophoretically trapped at the gap between the nanoelectrodes are able to rotate; as elaborated above, molecular subdomains must be at close proximity to the strong electric field near the nanogap in order to yield a measurable Raman signal. It has been shown that the Clausius-Mossotti-Factor of non-spherical objects depends on their orientation in the electric field.[64] We therefore conclude that the (non-spherical) Aβ peptide in the DEP field will tend to minimize its energy by adopting an

orientation with respect to the shared DEP and Raman hotspot that maximizes the DEP interaction, which explains the presence or absence of Raman signatures of various subdomains prone to be located near to or far from the hotspot region, respectively. In contrast, for the measurement in dried state, the sample was drop casted over the nanogap chip and dried in the desiccator prior to the experiment without applying the trapping field, therefore the peptides should have no preferred orientation.[46]

CONCLUSIONS

In summary, it has been shown in this study that the combination of DEP and SERS may serve as a novel and powerful tool for protein conformation studies, with the DEP force controlling the molecular orientation in the hotspot enabling the acquisition of more consistent SERS spectra from repeated experiments than most other techniques. Using our platform, experiments under identical conditions can be repeated on the same SERS hot spot in an identical target solution, potentially yielding SERS spectra with different features of the target enhanced within the same experiment, where all parameters are the same except the positioning of the target molecule within the hotspot. The increased SERS sensitivity of the Au nanoelectrodes enables clear distinction of features in the Raman spectrum while the DEP force provides a method to trap and detect peptides in solution without further modification, thus preserving their natural state and bioactivity. The DEP force can be tuned by different means, enabling the selection of molecules trapped in time-average. In this way, it can be made sure to acquire data from a low copy-number of the desired target molecules in solution phase originating from a heterogeneous sample. This eliminates issues of the experiments using dried samples on roughened surfaces, and renders information from the

molecular conformation and kinetics. Therefore, this new approach is superior to methods that result in random target orientation, such as drop-casting and spin-coating or mixing suspended plasmonic nanoparticles with the sample solution. Here, we have demonstrated that this technique is capable of distinguishing aggregates from monomers by comparing the phenylalanine signal in solution phase, while fibrils can be distinguished from other aggregates via amide bands in our SERS data. Results from previous work could be corroborated through analysis of the amide III and phenylalanine bands, confirming that Aβ peptides in the absence of Zn^{2+} aggregate by forming β-sheet abundant fibrils, whereas Aβ peptides in the presence of Zn^{2+} show signature of aggregation without β-sheet formation and therefore without fibrillization. The capability of this platform to study and distinguish different conformations of peptides, when combined with the ability to selectively capture peptides with different sizes, opens up possibilities for multiple future applications. Regarding Alzheimer's disease, this platform showed for the first time to provide spectroscopic structural information in physiological concentration since Aβ in plasma and cerebral spinal fluids is in sub-nanomolar range[65, 66]. This platform could serve as a diagnostic tool for Aβ as a biomarker, if further coupled to fluidic channels and specific bioconjugation approaches, or it might be used for the screening of novel therapeutic drugs, such as zinc chelators which have recently been found to restore Aβ fibrillization leading to the production of the less neurotoxic fibrils.[3] Being the real-time spectroscopic observation of oligomer/fibril formation in the early stages (from monomers) and a totally different experiment from the one over prolonged aggregation stages described in our manuscript, one could envision the observation of the oligomer formation kinetics from the spectroscopic data. The technology can further facilitate the understanding and characterization of heterogenous oligomers/aggregates in a plethora of neurodegenerative diseases, not limited to Aβ and Alzheimer's disease.

METHODS

Device fabrication and characterization. E-beam lithography and e-gun evaporation with a subsequent lift-off process were used to fabricate the nanostructures of our device. The platform for this experiment is fabricated on a 7mm x 7mm silicon substrate with a 1μm SiO_2 layer. The pattern for the microwire structure is defined by UV lithography. RIE etching 50-100nm into the surface before subsequent e-gun deposition of a Ti/Au double layer equal in thickness to the etching depth and lift-off of excess material ensures that the resulting electrode surface is even with the surrounding substrate. Following this, the nanoelectrode structure is defined by e-beam writing in alignment with the microelectrodes. In the same way, we fabricated marks on the chip which indicate the location of each nanogap. Analogously to the process described above, the electrode material is fabricated by e-gun deposition of a Ti/Au double layer in a thickness of 40nm and subsequent lift-off. Every chip was inspected by scanning electron microscopy (SEM, FEI Nova) with acceleration voltage of 10 kV, 0.54 nA, and a working distance of 5 mm to look for fabrication defects, determine the dimensions and confirm the quality of each nanogap.

DEP trapping. A custom-made printed circuit board with signal amplification, filtration and data acquisition capabilities with 0.02 nA current measurement resolution and 1 ms temporal resolution was used. To avoid interference of low-frequency field induced electrohydrodynamic flow with the DEP force, as discussed in our previous publication [18], trapping was performed using high-frequency AC field (1-3 MHz), which was applied by a function generator (33220A, Agilent) and monitored by an oscilloscope.

Aβ synthesis and preparation. Aβ40 peptides were synthesized using Fmoc (N-(9-fluorenyl)methoxycarbonyl solid phase chemistry by the peptide synthesis core of Genomics Research Center, Academia Sinica, Taiwan and further purified by reverse phase high performance liquid chromatography as previously described.[3, 67-70] Aβ peptides were dissolved in 1,1,1,3,3,3-Hexafluoro-2-propanol (HFIP, Sigma-Aldrich, St. Louis, MO, USA) in 1 mg/mL to dissolve preformed aggregates. The solution was lyophilized, then treated with 10% NH4OH and lyophilized again. Finally, lyophilized Aβ40 was dissolved in 10 mM Tris-HCl buffer, pH 7.4. The 50 μM Aβ solution was prepared in the presence or absence of 50 μM Zn^{2+}. The samples were incubated for 0, 43, 79 and 144 hours at 25 ℃ with agitating 60 seconds per hour, then diluted to the final concentration of 50 nM in deionized water for Raman experiments. For fluorescence observations, the FAM-Aβ42 was purchased from Biopeptide (San Diego, CA, USA). FAM-Aβ42 oligomers were prepared following the protocol for producing Aβ-derived diffusible ligand, ADDL.[71] Briefly, 5 mM of FAM-Aβ42 was prepared in anhydrous DMSO and diluted to 100 μM using Ham's F12 medium. The solution was further quiescently incubated at 4 °C for 1 day. Oligomeric FAM-Aβ42 was aliquoted, frozen by liquid nitrogen, and stored at -20 °C for later use. For experiments, a droplet of 1μL sample solution was placed on the center of the chip and encapsulated by a small fluidic chamber defined in 70 μm thick double-sided tape with a circular coverslip of 5 mm diameter (Knittel Glaeser) on top.

Fluorescence microscopy. Images were acquired using an inverted fluorescence microscope (Leica DMI6000) with a LED lamp as light source and a K3 filter cube (Ex/Em: BP 470−490 nm/LP 515, Leica). A 100x oil-immersion objective (Leica, N.A. 1.4), and an EMCCD camera (IXon-888, Andor Technologies) were used for the observations.

Raman measurements. Raman spectra were obtained using a WITec alpha300 confocal Raman microscope with a 640 nm excitation laser. A 100x air objective (N.A. 0.9) was used to deliver 1-2 mW laser power after the objective to the sample with an approximate spotsize of 1 μm. The recorded wavenumber axis was calibrated for each spectrum by setting the Si phonon peak to 520 cm^{-1}. All peak wavenumbers are reported with an error of ±3 cm^{-1}. The polarization of the laser light was aligned to be parallel to the nanoelectrode axis and spectra were taken with 10 s integration time. SERS spectra of Aβ40 were taken in aqueous solution in the presence and absence of Zn^{2+}, each at four different stages of aggregation, namely after 0, 43, 79 and 144 hours. All spectra have been background subtracted and normalized to the C-C-N stretching mode at 1144 cm^{-1}. Each Raman spectrum of a single aggregation stage is averaged over three measurements.

ThT Assay. A 50 μM Aβ solution was prepared in the presence of 5 μM Thioflavin T (ThT, Sigma-Aldrich, St. Louis, MO) as previously described.[69] Briefly, the samples were incubated at 25 °C with agitating 60 seconds per hour. Fluorescence of ThT was monitored at 485 nm by an ELISA microplate reader SpectraMax M5 (Molecular Devices, Sunnyvale, CA, USA), with an excitation wavelength of 442 nm. The experiments were repeated at least 3 times, averaged and presented as mean ± S.D.

AUTHOR INFORMATION

Contributions

L.L-R. and C.F.C. conceived the study; G.H. fabricated the device; M.L.C. designed the electronics and PCB interface; M.C.L., Y.J.C. and Y.R.C. prepared the Aβ samples, performed biochemical characterization and TEM images; K.H.P.V. performed DEP trapping, fluorescence

imaging, and SERS measurements; K.H.P.V. analyzed data with L.L-R. and A.E.; K.H.P.V., G.H., Y.R.C., L.L-R., A.E. and C.F.C. wrote the paper.

Corresponding Authors

*E-mail: cfchou@phys.sinica.edu.tw; yrchen@gate.sinica.edu.tw

ETHICS DECLARATIONS

Competing interests

The authors declare no competing financial interest.

ACKNOWLEDGMENT

We thank Academia Sinica Nano Core Facilities for technical assistance. This work is supported by Academia Sinica (grant# AS-TP-106-ML03, CDA-106-L01, and AS-IA-109-M04) and Ministry of Science and Technology (MOST), Taiwan, R.O.C. (grant# 107-2923-M-001-011-MY3, 108-2119-M-001-017, and 109-2124-M-001-003).

Supporting Information

The Supporting Information is available online free of charge on the ACS Publications website. Experimental setup, two movies (Movies S1 and S2) and a figure accompanying Figure 2 showing the reversible trapping of FAM-labelled-Aβ oligomers, and extra SERS spectra of Aβ and MgAβ.

REFERENCES

1. McKhann, G.; Drachman, D.; Folstein, M.; Katzman, R.; Price, D.; Stadlan, E. M., Clinical diagnosis of Alzheimer's disease: report of the NINCDS-ADRDA Work Group under the auspices of Department of Health and Human Services Task Force on Alzheimer's Disease. *Neurology* **1984,** *34* (7), 939-44.

2. Lutz, W.; Sanderson, W.; Scherbov, S., The coming acceleration of global population ageing. *Nature* **2008,** *451*, 716.
3. Lee, M. C.; Yu, W. C.; Shih, Y. H.; Chen, C. Y.; Guo, Z. H.; Huang, S. J.; Chan, J. C. C.; Chen, Y. R., Zinc ion rapidly induces toxic, off-pathway amyloid-beta oligomers distinct from amyloid-beta derived diffusible ligands in Alzheimer's disease. *Sci Rep* **2018,** *8* (1), 4772.
4. Selkoe, D. J.; Hardy, J., The amyloid hypothesis of Alzheimer's disease at 25 years. *EMBO Mol Med* **2016,** *8* (6), 595-608.
5. Masters, C. L.; Simms, G.; Weinman, N. A.; Multhaup, G.; McDonald, B. L.; Beyreuther, K., Amyloid plaque core protein in Alzheimer disease and Down syndrome. *Proc Natl Acad Sci U S A* **1985,** *82* (12), 4245-9.
6. Roychaudhuri, R.; Yang, M.; Hoshi, M. M.; Teplow, D. B., Amyloid beta-protein assembly and Alzheimer disease. *J Biol Chem* **2009,** *284* (8), 4749-53.
7. Sengupta, U.; Nilson, A. N.; Kayed, R., The Role of Amyloid-beta Oligomers in Toxicity, Propagation, and Immunotherapy. *EBioMedicine* **2016,** *6*, 42-49.
8. Bush, A. I., Copper, zinc, and the metallobiology of Alzheimer disease. *Alzheimer Dis Assoc Disord* **2003,** *17* (3), 147-50.
9. Zatta, P.; Drago, D.; Bolognin, S.; Sensi, S. L., Alzheimer's disease, metal ions and metal homeostatic therapy. *Trends Pharmacol Sci* **2009,** *30* (7), 346-55.
10. Minicozzi, V.; Stellato, F.; Comai, M.; Dalla Serra, M.; Potrich, C.; Meyer-Klaucke, W.; Morante, S., Identifying the minimal copper- and zinc-binding site sequence in amyloid-beta peptides. *J Biol Chem* **2008,** *283* (16), 10784-92.
11. Noy, D.; Solomonov, I.; Sinkevich, O.; Arad, T.; Kjaer, K.; Sagi, I., Zinc-amyloid beta interactions on a millisecond time-scale stabilize non-fibrillar Alzheimer-related species. *J Am Chem Soc* **2008,** *130* (4), 1376-83.
12. Tougu, V.; Karafin, A.; Zovo, K.; Chung, R. S.; Howells, C.; West, A. K.; Palumaa, P., Zn(II)- and Cu(II)-induced non-fibrillar aggregates of amyloid-beta (1-42) peptide are transformed to amyloid fibrils, both spontaneously and under the influence of metal chelators. *J Neurochem* **2009,** *110* (6), 1784-95.
13. Chen, W. T.; Liao, Y. H.; Yu, H. M.; Cheng, I. H.; Chen, Y. R., Distinct effects of Zn2+, Cu2+, Fe3+, and Al3+ on amyloid-beta stability, oligomerization, and aggregation: amyloid-beta destabilization promotes annular protofibril formation. *J Biol Chem* **2011,** *286* (11), 9646-56.
14. Solomonov, I.; Korkotian, E.; Born, B.; Feldman, Y.; Bitler, A.; Rahimi, F.; Li, H.; Bitan, G.; Sagi, I., Zn2+-Abeta40 complexes form metastable quasi-spherical oligomers that are cytotoxic to cultured hippocampal neurons. *J Biol Chem* **2012,** *287* (24), 20555-64.
15. Siddhanta, S.; Narayana, C., Surface Enhanced Raman Spectroscopy of Proteins: Implications for Drug Designing. *Nanomater Nanotechnol* **2012,** *2*, 1.
16. Rygula, A.; Majzner, K.; Marzec, K. M.; Kaczor, A.; Pilarczyk, M.; Baranska, M., Raman spectroscopy of proteins: a review. *J Raman Spectrosc* **2013,** *44* (8), 1061-1076.
17. Kneipp, K.; Kneipp, H.; Irving, I.; Ramachandra, R. D.; Michael, S. F., Surface-enhanced Raman scattering and biophysics. *Journal of Physics: Condensed Matter* **2002,** *14* (18), R597.
18. Langer, J.; Jimenez de Aberasturi, D.; Aizpurua, J.; Alvarez-Puebla, R. A.; Auguié, B.; Baumberg, J. J.; Bazan, G. C.; Bell, S. E. J.; Boisen, A.; Brolo, A. G.; Choo, J.; Cialla-May, D.; Deckert, V.; Fabris, L.; Faulds, K.; García de Abajo, F. J.; Goodacre, R.; Graham, D.; Haes, A. J.; Haynes, C. L.; Huck, C.; Itoh, T.; Käll, M.; Kneipp, J.; Kotov, N. A.; Kuang, H.; Le Ru, E. C.; Lee, H. K.; Li, J.-F.; Ling, X. Y.; Maier, S. A.; Mayerhöfer, T.; Moskovits, M.; Murakoshi, K.; Nam, J.-M.; Nie, S.; Ozaki, Y.; Pastoriza-Santos, I.; Perez-Juste, J.; Popp, J.; Pucci, A.; Reich,

S.; Ren, B.; Schatz, G. C.; Shegai, T.; Schlücker, S.; Tay, L.-L.; Thomas, K. G.; Tian, Z.-Q.; Van Duyne, R. P.; Vo-Dinh, T.; Wang, Y.; Willets, K. A.; Xu, C.; Xu, H.; Xu, Y.; Yamamoto, Y. S.; Zhao, B.; Liz-Marzán, L. M., Present and Future of Surface-Enhanced Raman Scattering. *ACS Nano* **2020**, *14 (1)*, 28-117.
19. Hess, C., New advances in using Raman spectroscopy for the characterization of catalysts and catalytic reactions. *Chem Soc Rev* **2021,** *50* (5), 3519-3564.
20. Moskovits, M.; Piorek, B. D., A brief history of surface-enhanced Raman spectroscopy and the localized surface plasmon Dedicated to the memory of Richard Van Duyne (1945–2019). *Journal of Raman Spectroscopy* **2021,** *52* (2), 279-284.
21. Mahler, H. C.; Friess, W.; Grauschopf, U.; Kiese, S., Protein aggregation: pathways, induction factors and analysis. *J Pharm Sci* **2009,** *98* (9), 2909-34.
22. Pohl, H. A., *Dielectrophoresis : the behavior of neutral matter in nonuniform electric fields*. Cambridge University Press: Cambridge; New York, 1978.
23. Pethig, R., Review article-dielectrophoresis: status of the theory, technology, and applications. *Biomicrofluidics* **2010**, *4* (2) 22811.
24. Pethig, R., *Dielectrophoresis : theory, methodology, and biological applications*. Hoboken, NJ : John Wiley & Sons, Inc.: USA, 2017.
25. Chou, C. F.; Tegenfeldt, J. O.; Bakajin, O.; Chan, S. S.; Cox, E. C.; Darnton, N.; Duke, T.; Austin, R. H., Electrodeless dielectrophoresis of single- and double-stranded DNA. *Biophys J* **2002,** *83* (4), 2170-9.
26. Chou, C. F.; Zenhausern, F., Electrodeless dielectrophoresis for micro total analysis systems. *IEEE Eng Med Biol Mag* **2003,** *22* (6), 62-7.
27. Liao, K. T.; Chou, C. F., Nanoscale molecular traps and dams for ultrafast protein enrichment in high-conductivity buffers. *J Am Chem Soc* **2012,** *134* (21), 8742-5.
28. Rohani, A.; Sanghavi, B. J.; Salahi, A.; Liao, K. T.; Chou, C. F.; Swami, N. S., Frequency-selective electrokinetic enrichment of biomolecules in physiological media based on electrical double-layer polarization. *Nanoscale* **2017,** *9* (33), 12124-12131.
29. Swami, N.; Chou, C. F.; Ramamurthy, V.; Chaurey, V., Enhancing DNA hybridization kinetics through constriction-based dielectrophoresis. *Lab Chip* **2009,** *9* (22), 3212-20.
30. Sanghavi, B. J.; Varhue, W.; Chavez, J. L.; Chou, C. F.; Swami, N. S., Electrokinetic preconcentration and detection of neuropeptides at patterned graphene-modified electrodes in a nanochannel. *Anal Chem* **2014,** *86* (9), 4120-5.
31. Hatab, N. A.; Hsueh, C. H.; Gaddis, A. L.; Retterer, S. T.; Li, J. H.; Eres, G.; Zhang, Z.; Gu, B., Free-standing optical gold bowtie nanoantenna with variable gap size for enhanced Raman spectroscopy. *Nano Lett* **2010,** *10* (12), 4952-5.
32. Dodson, S.; Haggui, M.; Bachelot, R.; Plain, J.; Li, S.; Xiong, Q., Optimizing Electromagnetic Hotspots in Plasmonic Bowtie Nanoantennae. *J Phys Chem Lett* **2013,** *4* (3), 496-501.
33. Ding, W.; Bachelot, R.; Kostcheev, S.; Royer, P.; Espiau de Lamaestre, R., Surface plasmon resonances in silver Bowtie nanoantennas with varied bow angles. *Journal of Applied Physics* **2010,** *108* (12), 124314.
34. Lesser-Rojas, L.; Ebbinghaus, P.; Vasan, G.; Chu, M.-L.; Erbe, A.; Chou, C.-F., Low-Copy Number Protein Detection by Electrode Nanogap-Enabled Dielectrophoretic Trapping for Surface-Enhanced Raman Spectroscopy and Electronic Measurements. *Nano Letters* **2014,** *14* (5), 2242-2250.

35. Albrecht, G.; Ubl, M.; Kaiser, S.; Giessen, H.; Hentschel, M., Comprehensive Study of Plasmonic Materials in the Visible and Near-Infrared: Linear, Refractory, and Nonlinear Optical Properties. *ACS Photonics* **2018,** *5* (3), 1058-1067.
36. Arosio, P.; Knowles, T. P.; Linse, S., On the lag phase in amyloid fibril formation. *Phys Chem Chem Phys* **2015,** *17* (12), 7606-18.
37. Clement, J. E.; Leray, A.; Bouhelier, A.; Finot, E., Spectral pointillism of enhanced Raman scattering for accessing structural and conformational information on single protein. *Phys Chem Chem Phys* **2016,** *19* (1), 458-466.
38. Chou, I. H.; Benford, M.; Beier, H. T.; Cote, G. L.; Wang, M.; Jing, N.; Kameoka, J.; Good, T. A., Nanofluidic biosensing for beta-amyloid detection using surface enhanced Raman spectroscopy. *Nano Lett* **2008,** *8* (6), 1729-35.
39. Choi, I.; Huh, Y. S.; Erickson, D. J. M.; Ultra-sensitive, label-free probing of the conformational characteristics of amyloid beta aggregates with a SERS active nanofluidic device. *Microfluid Nanofluid* **2012**, *12* (1), 663-669.
40. Wang, Q.; Wang, Y.; Lu, H. P., Revealing the secondary structural changes of amyloid β peptide by probing the spectral fingerprint characters. *J Raman Spectrosc* **2013**, *44* (5), 670-674.
41. Dong, J.; Atwood, C. S.; Anderson, V. E.; Siedlak, S. L.; Smith, M. A.; Perry, G.; Carey, P. R., Metal binding and oxidation of amyloid-beta within isolated senile plaque cores: Raman microscopic evidence. *Biochemistry* **2003,** *42* (10), 2768-73.
42. Miura, T.; Suzuki, K.; Kohata, N.; Takeuchi, H., Metal binding modes of Alzheimer's amyloid beta-peptide in insoluble aggregates and soluble complexes. *Biochemistry* **2000,** *39* (23), 7024-31.
43. Kurouski, D.; Van Duyne, R. P.; Lednev, I. K., Exploring the structure and formation mechanism of amyloid fibrils by Raman spectroscopy: a review. *Analyst* **2015,** *140* (15), 4967-80.
44. Maiti, N. C.; Apetri, M. M.; Zagorski, M. G.; Carey, P. R.; Anderson, V. E., Raman spectroscopic characterization of secondary structure in natively unfolded proteins: alpha-synuclein. *J Am Chem Soc* **2004,** *126* (8), 2399-408.
45. Lippert, J. L.; Gorczyca, L. E.; Meiklejohn, G., A laser Raman spectroscopic investigation of phospholipid and protein configurations in hemoglobin-free erythrocyte ghosts. *Biochim Biophys Acta* **1975,** *382* (1), 51-7.
46. Blum, C.; Schmid, T.; Opilik, L.; Metanis, N.; Weidmann, S.; Zenobi, R., Missing Amide I Mode in Gap-Mode Tip-Enhanced Raman Spectra of Proteins. *The Journal of Physical Chemistry C* **2012,** *116* (43), 23061-23066.
47. Holzel, R.; Calander, N.; Chiragwandi, Z.; Willander, M.; Bier, F. F., Trapping single molecules by dielectrophoresis. *Phys Rev Lett* **2005,** *95* (12), 128102.
48. Schwille, P., Fluorescence correlation spectroscopy and its potential for intracellular applications. *Cell Biochem Biophys* **2001,** *34* (3), 383-408.
49. Kirkwood, J. G.; Goldberg, R. J., Light Scattering Arising from Composition Fluctuations in Multi-Component Systems. *The Journal of Chemical Physics* **1950,** *18* (1), 54-57.
50. Elson, E. L.; Magde, D., Fluorescence correlation spectroscopy. I. Conceptual basis and theory. *Biopolymers* **1974,** *13* (1), 1-27.
51. Sereda, V.; Lednev, I. K., Two Mechanisms of Tip Enhancement of Raman Scattering by Protein Aggregates. *Appl Spectrosc* **2017**, *71* (1), 118-128.

52. Kurouski, D.; Postiglione, T.; Deckert-Gaudig, T.; Deckert, V.; Lednev, I. K., Amide I vibrational mode suppression in surface (SERS) and tip (TERS) enhanced Raman spectra of protein specimens. *Analyst* **2013,** *138* (6), 1665-73.
53. Groenning, M., Binding mode of Thioflavin T and other molecular probes in the context of amyloid fibrils-current status. *J Chem Biol* **2010,** *3* (1), 1-18.
54. Tycko, R., Molecular structure of amyloid fibrils: insights from solid-state NMR. *Q Rev Biophys* **2006,** *39* (1), 1-55.
55. Xu, M.; Ermolenkov, V. V.; Uversky, V. N.; Lednev, I. K., Hen egg white lysozyme fibrillation: a deep-UV resonance Raman spectroscopic study. *J Biophotonics* **2008,** *1* (3), 215-29.
56. Kurouski, D.; Deckert-Gaudig, T.; Deckert, V.; Lednev, I. K., Structure and composition of insulin fibril surfaces probed by TERS. *J Am Chem Soc* **2012,** *134* (32), 13323-9.
57. Xu, M.; Ermolenkov, V. V.; He, W.; Uversky, V. N.; Fredriksen, L.; Lednev, I. K., Lysozyme fibrillation: deep UV Raman spectroscopic characterization of protein structural transformation. *Biopolymers* **2005,** *79* (1), 58-61.
58. Tabatabaei, M.; Caetano, F. A.; Pashee, F.; Ferguson, S. S. G.; Lagugne-Labarthet, F., Tip-enhanced Raman spectroscopy of amyloid beta at neuronal spines. *Analyst* **2017,** *142* (23), 4415-4421.
59. David, C.; Guillot, N.; Shen, H.; Toury, T.; de la Chapelle, M. L., SERS detection of biomolecules using lithographed nanoparticles towards a reproducible SERS biosensor. *Nanotechnology* **2010,** *21* (47), 475501.
60. Podstawka, E.; Sikorska, E.; Proniewicz, L. M.; Lammek, B., Raman and surface-enhanced Raman spectroscopy investigation of vasopressin analogues containing 1-aminocyclohexane-1-carboxylic acid residue. *Biopolymers* **2006,** *83* (2), 193-203.
61. Stiles, P. L.; Dieringer, J. A.; Shah, N. C.; Van Duyne, R. P., Surface-enhanced Raman spectroscopy. *Annu Rev Anal Chem (Palo Alto Calif)* **2008,** *1*, 601-26.
62. Baumketner, A.; Bernstein, S. L.; Wyttenbach, T.; Bitan, G.; Teplow, D. B.; Bowers, M. T.; Shea, J. E., Amyloid beta-protein monomer structure: a computational and experimental study. *Protein Sci* **2006,** *15* (3), 420-8.
63. Fabian, H.; Anzenbacher, P., New developments in Raman spectroscopy of biological systems. *Vibrational Spectroscopy* **1993,** *4* (2), 125-148.
64. Yang, C. Y.; Lei, U., Quasistatic force and torque on ellipsoidal particles under generalized dielectrophoresis. *J Appl Phys* **2007**, *102* (9), 094702.
65. Ovod, V.; Ramsey, K. N.; Mawuenyega, K. G.; Bollinger, J. G.; Hicks, T.; Schneider, T.; Sullivan, M.; Paumier, K.; Holtzman, D. M.; Morris, J. C.; Benzinger, T.; Fagan, A. M.; Patterson, B. W.; Bateman, R. J., Amyloid beta concentrations and stable isotope labeling kinetics of human plasma specific to central nervous system amyloidosis. *Alzheimers Dement* **2017,** *13* (8), 841-849.
66. Lewczuk, P.; Lelental, N.; Spitzer, P.; Maler, J. M.; Kornhuber, J., Amyloid-beta 42/40 cerebrospinal fluid concentration ratio in the diagnostics of Alzheimer's disease: validation of two novel assays. *J Alzheimers Dis* **2015,** *43* (1), 183-91.
67. Chen, Y. R.; Glabe, C. G., Distinct early folding and aggregation properties of Alzheimer amyloid-beta peptides Abeta40 and Abeta42: stable trimer or tetramer formation by Abeta42. *J Biol Chem* **2006,** *281* (34), 24414-22.

68. Burdick, D.; Soreghan, B.; Kwon, M.; Kosmoski, J.; Knauer, M.; Henschen, A.; Yates, J.; Cotman, C.; Glabe, C., Assembly and aggregation properties of synthetic Alzheimer's A4/beta amyloid peptide analogs. *J Biol Chem* **1992,** *267* (1), 546-54.
69. Chang, Y. J.; Chen, Y. R., The coexistence of an equal amount of Alzheimer's amyloid-beta 40 and 42 forms structurally stable and toxic oligomers through a distinct pathway. *FEBS J* **2014,** *281* (11), 2674-87.
70. Lin, T. W.; Chang, C. F.; Chang, Y. J.; Liao, Y. H.; Yu, H. M.; Chen, Y. R., Alzheimer's amyloid-beta A2T variant and its N-terminal peptides inhibit amyloid-beta fibrillization and rescue the induced cytotoxicity. *PLoS One* **2017,** *12* (3), e0174561.
71. Lambert, M. P.; Barlow, A. K.; Chromy, B. A.; Edwards, C.; Freed, R.; Liosatos, M.; Morgan, T. E.; Rozovsky, I.; Trommer, B.; Viola, K. L.; Wals, P.; Zhang, C.; Finch, C. E.; Krafft, G. A.; Klein, W. L., Diffusible, nonfibrillar ligands derived from Abeta1-42 are potent central nervous system neurotoxins. *Proc Natl Acad Sci U S A* **1998,** *95* (11), 6448-53.

For Table of Contents Only (TOC Graphic)